JBC RESEARCH ARTICLE

NOTCH2 promotes osteoclast maturation and metabolism and modulates the transcriptome profile during osteoclastogenesis

Received for publication, November 9, 2023, and in revised form, December 11, 2023 Published, Papers in Press, December 28, 2023,
https://doi.org/10.1016/j.jbc.2023.105613

Ernesto Canalis[1,2,3,*], **Lauren Schilling**[3], **Jungeun Yu**[1,3], **and Emily Denker**[3]

From the [1]*Department of Orthopaedic Surgery,* [2]*Department of Medicine, and* [3]*UConn Musculoskeletal Institute, UConn Health, Farmington, Connecticut, USA*

Reviewed by members of the JBC Editorial Board. Edited by Robert Haltiwanger

Notch signaling plays a key regulatory role in bone remodeling and NOTCH2 enhances osteoclastogenesis, an effect that is mostly mediated by its target gene *Hes1*. In the present study, we explored mechanisms responsible for the enhanced osteoclastogenesis in bone marrow–derived macrophages (BMM) from *Notch2*$^{tm1.1Ecan}$, harboring a NOTCH2 gain-of-function mutation, and control mice. *Notch2*$^{tm1.1Ecan}$ mice are osteopenic and have enhanced osteoclastogenesis. Bulk RNA-Seq and gene set enrichment analysis of *Notch2*$^{tm1.1Ecan}$ BMMs cultured in the presence of macrophage colony stimulating factor (M-CSF) and receptor activator of NF-κB ligand revealed enrichment of genes associated with enhanced cell metabolism, aerobic respiration, and mitochondrial function, all associated with osteoclastogenesis. These pathways were not enhanced in the context of a *Hes1* inactivation. Analysis of single cell RNA-Seq data of pooled control and *Notch2*$^{tm1.1Ecan}$ BMMs treated with M-CSF or M-CSF and receptor activator of NF-κB ligand for 3 days identified 11 well-defined cellular clusters. Pseudotime trajectory analysis indicated a trajectory of clusters expressing genes associated with osteoclast progenitors, osteoclast precursors, and mature cells. There were an increased number of cells expressing gene markers associated with the osteoclast and with an unknown, albeit related, cluster in *Notch2*$^{tm1.1Ecan}$ than in control BMMs as well as enhanced expression of genes associated with osteoclast progenitors and precursors in *Notch2*$^{tm1.1Ecan}$ cells. In conclusion, BMM cultures display cellular heterogeneity, and NOTCH2 enhances osteoclastogenesis, increases mitochondrial and metabolic activity of osteoclasts, and affects cell cluster allocation in BMMs.

Notch receptors (Notch 1 and 4) play an important and distinct role in osteoclast differentiation and function (1–6). Whereas NOTCH1 has direct and indirect inhibitory effects on osteoclastogenesis, NOTCH2 and NOTCH3 enhance osteoclast differentiation (1, 5, 7, 8). NOTCH3 acts by inducing the expression of receptor activator of NF-κB ligand (RANKL) by cells of the osteoblast lineage, whereas NOTCH2 induces RANKL and also acts directly on myeloid precursors modulating their differentiation into osteoclasts (6–8). Importantly, NOTCH1 and NOTCH2 are the Notch receptors preferentially expressed by cells of the osteoclast lineage substantiating their relevance to the differentiation and function of these cells (2, 3).

The activation of Notch follows interactions of its extracellular domain with ligands of the Jagged and Delta-like families leading to the exposure of the negative regulatory region (NRR) to the activity of ADAM metalloproteases and the γ-secretase complex (9, 10). This results in the proteolytic cleavage of the NRR and the release of the Notch intracellular domain (NICD) (11). The NICD translocates to the nucleus to form a complex with recombination signal-binding protein for immunoglobulin kappa J region and mastermind-like to induce target gene transcription (10, 12–14). Genes targeted by this canonical pathway are members of the Hairy Enhancer of Split (*Hes*) and Hes-related with YRPW motif (*Hey*) families (15–17).

Our laboratory created a knock-in mouse model (*Notch2*$^{tm1.1Ecan}$) harboring a *Notch2*$^{6955C>T}$ mutation in exon 34 of *Notch2*, leading to the premature termination of a protein product lacking the PEST domain, which is necessary for the proteasomal degradation of the NOTCH2 NICD (4). This results in a stable NICD and a gain-of-NOTCH2 function (4). *Notch2*$^{tm1.1Ecan}$ mice exhibit the functional outcomes of the monogenic disorder Hajdu Cheney Syndrome, and hallmarks of the syndrome include bone loss and the presence of acro-osteolysis (18–22). *Notch2*$^{tm1.1Ecan}$ mice are osteopenic due to increased bone resorption and are sensitized to the effect of tumor necrosis factor α on osteolysis *in vivo* and the inflammatory response *in vitro* (7, 8, 23).

Hes1 and lower levels of *Hes3* and *Hes5* are detected in the myeloid/osteoclast lineage, whereas *Hey1*, *Hey2*, and *Heyl* are not, making *Hes1* the Notch target gene likely responsible for Notch activity in this lineage (8). Indeed, the inactivation of *Hes1* in *Ctsk*-expressing osteoclasts decreases their differentiation and bone resorbing capacity and ameliorates the osteopenic phenotype of *Notch2*$^{tm1.1Ecan}$mice (8). These observations indicate that HES1 is a primary effector of NOTCH2 signaling in osteoclasts. Accordingly, RNA-Seq

* For correspondence: Ernesto Canalis, canalis@uchc.edu.
Present address Jungeun Yu: Cellinfinity Bio, 520 West Campus Drive, West Haven, Connecticut 06030, USA.

analysis of HES1-activated osteoclasts revealed that HES1 modulates cell-to-cell fusion and bone resorbing capacity of osteoclasts. The signaling mechanisms and transcriptome profile affected by NOTCH2 at a single cell resolution in the myeloid/osteoclast lineage have not been explored. This is necessary since bone marrow–derived macrophages (BMM) exhibit transcriptomic heterogenicity during their differentiation to mature osteoclasts (24). Therefore, operational pathways during osteoclastogenesis are better defined at a single cell resolution.

To understand mechanisms involved in NOTCH2-dependent osteoclastogenesis, in the present study, we explored the transcriptome profile affected by a NOTCH2 gain-of-function in the myeloid/osteoclast lineage, during the differentiation of murine BMMs toward osteoclasts. To this end, transcriptomes of BMMs from *Notch2*$^{tm1.1Ecan}$ mutant mice were examined using bulk RNA as well as single cell RNA-Seq approaches during osteoclast differentiation.

Results

Hes1 is responsible for the enhanced NOTCH2-dependent osteoclastogenesis

To confirm the effect of NOTCH2 on osteoclastogenesis, BMM cultures from *Notch2*$^{tm1.1Ecan}$ mice were compared to cultures from control littermates. Following treatment with macrophage colony stimulating factor (M-CSF) and RANKL for 4 to 5 days, there was a significant increase in the number of osteoclasts in BMM cultures from *Notch2*$^{tm1.1Ecan}$ mice compared to littermate controls (Fig. 1). To determine the contributions of HES1 to the NOTCH2 phenotype, *Hes1* was inactivated in control and *Notch2*$^{tm1.1Ecan}$ *Ctsk*-expressing cells. To this end, BMMs derived from *Ctsk*$^{Cre/WT}$;*Hes1*$^{\Delta/\Delta}$ and control littermates were cultured in the presence of M-CSF and RANKL. *Ctsk*$^{Cre/WT}$;*Hes1*$^{\Delta/\Delta}$ cultures revealed a 20% decrease in osteoclast number when compared to cells from littermate controls (Fig. 1). Osteoclast number was decreased significantly (37%) in *Notch2*$^{tm1.1Ecan}$;*Hes1*$^{\Delta/\Delta}$ compared to *Notch2*$^{tm1.1Ecan}$ cells so that the *Hes1* inactivation reversed the enhanced osteoclastogenesis observed in the context of the *Notch2*$^{tm1.1Ecan}$ mutation, confirming that HES1 is a primary effector of NOTCH2 action in this cell lineage (8).

NOTCH2-dependent osteoclastogenesis is associated with enhanced mitochondrial function

To understand the molecular mechanisms associated with the effect of NOTCH2 on osteoclastogenesis, RNA from *Notch2*$^{tm1.1Ecan}$ and control BMMs treated with M-CSF and RANKL for 4 to 5 days was examined by bulk RNA-Seq analysis. Principal component analysis revealed clear separation between control and experimental samples (Fig. 2). Applying a false discovery rate (FDR) adjusted p value of 0.1, which denotes a relatively low threshold, there were 18 ≥ log2FC1 differentially regulated genes between *Notch2*$^{tm1.1Ecan}$ and control osteoclasts. Four genes, including *Il1b*, were upregulated in *Notch2*$^{tm1.1Ecan}$ osteoclasts and 14 were downregulated (Fig. 2, *C* and *D*) (Table S1). These included *Tnn* and *Tnc*, encoding tenascin N and C, *Csf1*, encoding M-CSF, *Timp3*, encoding tissue inhibitor of metalloproteases, and *Ccl12*, encoding cc motif chemokine ligand 12. Changes in mRNA expression were verified by real time reverse transcription polymerase chain reaction (RT-PCR) (Fig. S1). Gene set enrichment analysis (GSEA) of BMMs from *Notch2*$^{tm1.1Ecan}$ and control littermate mice cultured for 4 to 5 days with M-CSF and RANKL revealed enrichment of genes associated with enhanced metabolic and mitochondrial processes in *Notch2*$^{tm1.1Ecan}$ cells and known to be activated during osteoclastogenesis (25–29). These included genes associated with enhanced ATP synthesis, aerobic respiration, oxidative phosphorylation, and tricarboxylic acid cycle (Fig. 3*A*). Further functional gene enrichment analysis of biological pathways affected, using the R package clusterProfiler, confirmed activation of mitochondrial function and ATP synthesis, oxidative phosphorylation, and aerobic respiration in *Notch2*$^{tm1.1Ecan}$ osteoclasts as compared to control cells (Fig. 3*B*) (30, 31).

HES1 contributes to osteoclastogenesis

To understand the molecular mechanisms associated with the effect of HES1 on osteoclast differentiation in the context of the NOTCH2 gain-of-function, total RNA from *Notch2*$^{tm1.1Ecan}$;*Ctsk*$^{Cre/WT}$;*Hes1*$^{\Delta/\Delta}$ and control *Notch2*$^{tm1.1Ecan}$ osteoclasts was examined by RNA-Seq analysis. Principal component analysis revealed clear separation of sample groups (Fig. 4). There were modest changes in differentially expressed genes, but notably *Ctsk* was reduced in *Hes1*-deleted osteoclasts confirming the results obtained by RT-PCR (Fig. 1). In addition, the expression of *Xlr3b* that was increased in *Notch2*$^{tm1.1Ecan}$ osteoclasts, was inhibited by the *Hes1* deletion and the expression of *Tnn* that was inhibited in *Notch2*$^{tm1.1Ecan}$ osteoclasts was induced in *Hes1* deleted cells (Figs. 2, 4 and S1). GSEA revealed that metabolic processes associated with osteoclastogenesis were not enhanced in *Notch2*$^{tm1.1Ecan}$;*Ctsk*$^{Cre/WT}$;*Hes1*$^{\Delta/\Delta}$ osteoclasts. Functional gene enrichment analysis of molecular functions by clusterProfiler revealed decreased mitochondrial activity by the *Hes1* inactivation in *Notch2*$^{tm1.1Ecan}$ osteoclasts (not shown).

Single cell RNA-Seq reveals unique clusters in BMMs

Single cell RNA-Seq was conducted on control and *Notch2*$^{tm1.1Ecan}$ BMMs cultured on collagen gels in the presence of either M-CSF or M-CSF and RANKL for 3 days to avoid multinucleation and cell attachment. Under these conditions, BMMs differentiate in a manner analogous to when seeded on tissue culture plates but do not attach or become multinucleated, since this event requires treatment with M-CSF and RANKL for 4 to 5 days. Cells were processed in an Chromium iX using a 3′ library kit (10x Genomics). An estimated recovery of 21,886 cells among the four experimental groups was obtained. Normalization excluded cells with >10% mitochondrial RNA, cells with <250 transcripts and >10,000 genes/cell, as well as doublet filtering and exclusion, reducing the number of cells to be analyzed to 17,554. These cells included 4401 control and 2673 *Notch2*$^{tm1.1Ecan}$ BMMs treated

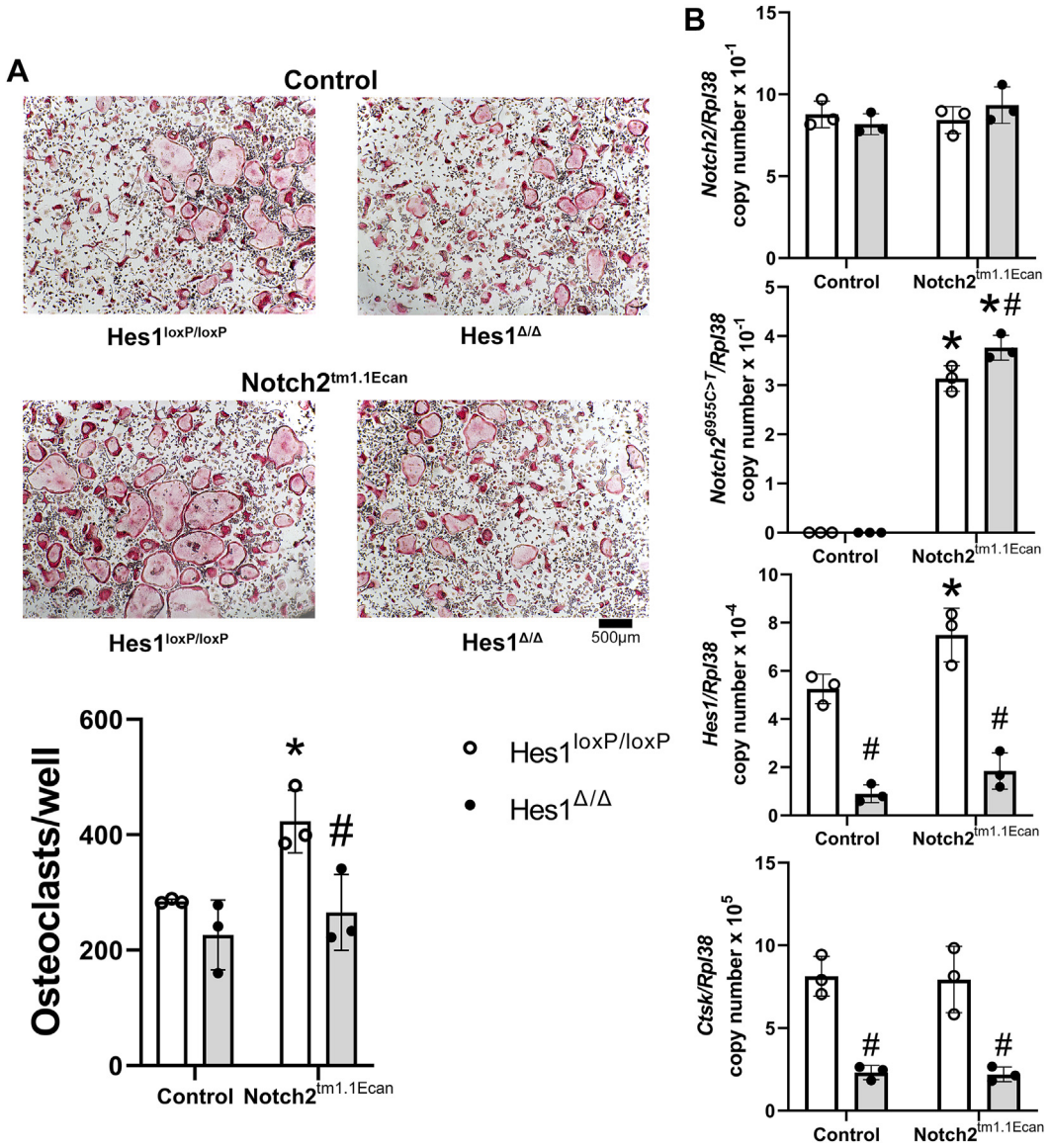

Figure 1. *Hes1* inactivation reverses the effect of NOTCH2 on osteoclastogenesis. Bone marrow–derived macrophages (BMM) from 7 to 8-week-old *Notch2*$^{tm1.1Ecan}$;*Ctsk*^{Cre};*Hes1*$^{Δ/Δ}$ and *Notch2*$^{tm1.1Ecan}$;*Hes1*$^{loxP/loxP}$ littermate controls were cultured for 4 to 5 days with M-CSF at 30 ng/ml and RANKL at 10 ng/ml until the formation of multinucleated TRAP-positive cells. *A*, representative images of TRAP-stained multinucleated cells are shown. The scale bar in the right corner represents 500 μm. TRAP-positive cells with more than 3 nuclei were considered osteoclasts and counted. *B*, total RNA was extracted, and gene expression determined by qRT-PCR. Data are expressed as *Notch2*, *Notch2*$^{6955C>T}$, *Hes1* and *Ctsk* corrected for *Rpl38* copy number. Values are means ± S.D; n = 3 technical replicates for control and *Notch2*$^{tm1.1Ecan}$ cells in the context of *Hes1*$^{loxP/loxP}$ (*white bar, open circles*) or *Hes1*$^{Δ/Δ}$ (*gray bar, black filled circles*) deleted alleles. *Significantly different between *Notch2*$^{tm1.1Ecan}$ and control, $p < 0.05$. #Significantly different between *Hes1*$^{Δ/Δ}$ and *Hes1*$^{loxP/loxP}$, $p < 0.05$ by 2-way ANOVA. M-CSF, macrophage colony stimulating factor; RANKL, receptor activator of NF-κB ligand.

with M-CSF and 4378 control and 6102 *Notch2*$^{tm1.1Ecan}$ BMMs treated with M-CSF and RANKL. The number of unique genes analyzed was 32,285. Clustering analysis of the pooled 17,554 cells from control and *Notch2*$^{tm1.1Ecan}$ BMMs, using uniform manifold approximation and projection (UMAP) for nonlinear dimensional reduction, accurately distinguished different cell types into clusters (32). Following data normalization, 19 cell clusters were identified (Table S2). The manual exclusion of clusters representing <1% of the cell population, except for osteoclasts, and the merging of clusters with analogous transcriptome identity resulted in a reduction of cells to 17,321 and the number of unique clusters to 11 (Fig. 5, Table 1). The complete list of 32,285 genes defining each cluster is shown in Table S3.

One of the clusters identified by the FindClusters function in Seurat expressed a gene profile associated with Memory CD8+ T-cells, dendritic cells, and progenitors and is termed progenitor, dendritic, CD8+ T cell cluster. Cells from this cluster expressed genes known to be associated with osteoclast progenitors, including *Cx3cr1*, *Cd74*, *H2-Aa*, *H2 -Ab1*, *H2-Eb1*, and *Itgax*, encoding *Cd11c*, was detected in a low number of cells (24, 33–36). Genes encoding osteoclast inhibitors, *Irf8, Bcl6*, and *Mafb*, are known to be expressed by osteoclast precursors and were mostly detected in the macrophage cluster, whereas

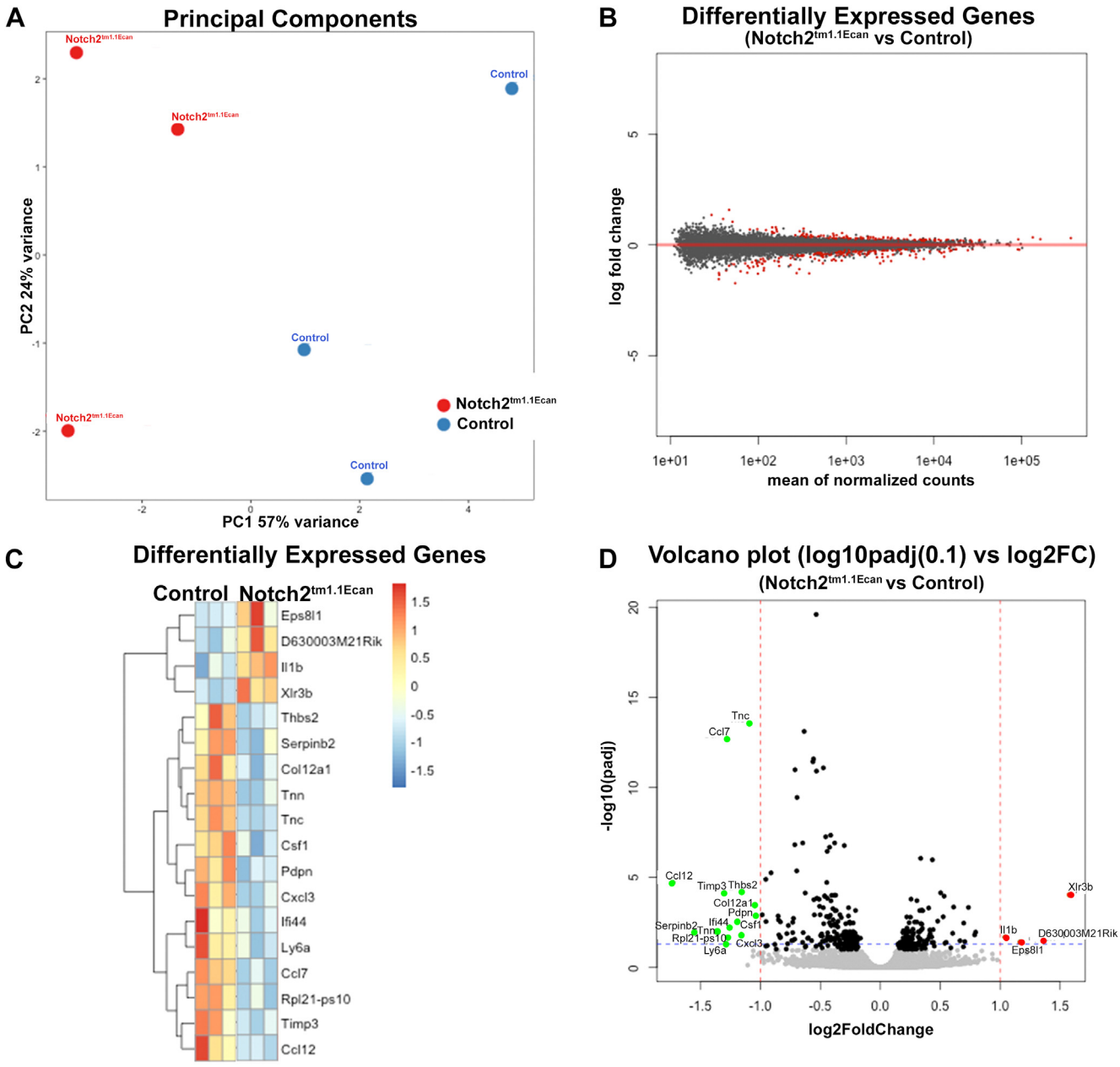

Figure 2. Transcriptional profile of *Notch2*$^{tm1.1Ecan}$ osteoclasts. Bone marrow–derived macrophages (BMM) from 7 to 8-week-old *Notch2*$^{tm1.1Ecan}$ (*Hes1*$^{loxP/loxP}$) mice and control (*Hes1*$^{loxP/loxP}$) littermates were cultured for 4 to 5 days in the presence of M-CSF at 30 ng/ml and RANKL at 10 ng/ml. Cells were collected for total RNA and analyzed by RNA-Seq. *A*, principal component (PC) analysis of RNA-Seq replicates (n = 3 for *Notch2*$^{tm1.1Ecan}$ and n = 3 for control). *B*, differentially expressed genes as log fold change over means of normalized counts. *C*, heat map and (*D*) volcano plots of differentially expressed genes between *Notch2*$^{tm1.1Ecan}$ (*Hes1*$^{loxP/loxP}$) and control (*Hes1*$^{loxP/loxP}$) osteoclasts, log2FC false discovery rate *p* adjusted value 0.1. M-CSF, macrophage colony stimulating factor; RANKL, receptor activator of NF-κB ligand.

Prdm1, encoding B-lymphocyte-induced maturation protein 1, a suppressor of these inhibitors, was found in the osteoclast cluster (37–39). Genes associated with mature osteoclasts, including *Acp5*, *Calcr*, *Oscar*, *Ctsk*, *DcStamp*, *OcStamp*, *Itgav*, *Mmp9*, *Nfatc1*, *Atp6vOd2*, and *Cited2* were used to identify what we named mature osteoclast cluster (Fig. 5) (24, 40, 41). *F2r*, a negative regulator of osteoclastogenesis, was expressed by a small percentage of cells from the osteoclast cluster (42). Confirming prior observations, *Notch1*, *Notch2*, and *Jag1* were expressed in the BMM cellular environment whereas *Notch3*, *Notch4*, *Dll1*, and *Dll4* were not present (Fig. 5) (3).

Pseudotime trajectory finding was constructed with Monocle 3 and was used to predict the differentiation trajectory among clusters (Fig. 6*A*). An alternate visualization using a boxplot of the pseudotime UMAP with the progenitor cluster as a route node revealed a closer association of the osteoclast mature cell than the precursor (macrophage) cluster to the progenitor cluster (Fig. 6*B*). Pseudotime trajectory finding selecting the clusters expressing osteoclast progenitors (Memory CD8+ T-cells), precursors (macrophage cluster), and mature cells confirmed an association among these clusters and a trajectory toward osteoclast maturation (Fig. 6*C*).

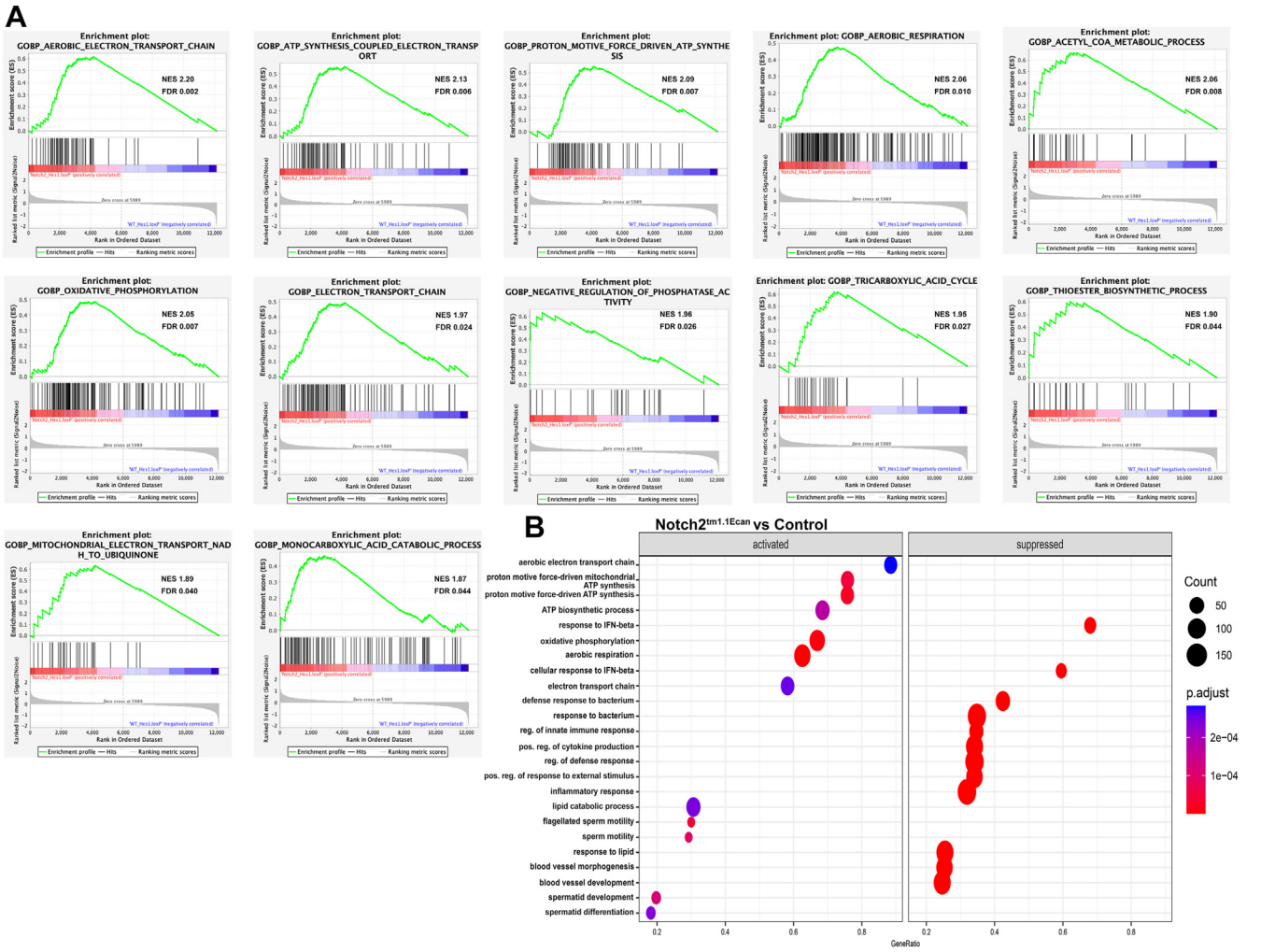

Figure 3. Mitochondrial activity and aerobic respiration are enhanced in *Notch2*$^{tm1.1Ecan}$ osteoclasts. *A*, gene set enrichment analysis of bone marrow–derived macrophages (BMM) from *Notch2*$^{tm1.1Ecan}$;*Hes1*$^{loxP/loxP}$ (n = 3) and control (*Hes1*$^{loxP/loxP}$) (n = 3) mice cultured in the presence of M-CSF at 30 ng/ml and RANKL at 10 ng/ml for 4 to 5 days. Enrichment scores (ES) and normalized ES (NES) of pathways affected by *Notch2*$^{tm1.1Ecan}$ osteoclasts at a false discovery ratio (FDR) of <0.05 are shown. *B*, visualization of gene enrichment analysis of *Notch2*$^{tm1.1Ecan}$ and control osteoclasts using clusterProfiler, shown as a lollipop chart. Gene count and pathways affected at a $p < 0.05$ are shown. M-CSF, macrophage colony stimulating factor; RANKL, receptor activator of NF-κB ligand.

In agreement with bulk RNA-Seq GSEA of *Notch2*$^{tm1.1Ecan}$ osteoclasts (Fig. 3), Ingenuity pathway analysis (IPA) of canonical pathways revealed increased mitochondrial function, oxidative phosphorylation, ATP synthesis, and electron transport in the osteoclast cluster (Fig. 7). It is of interest that these pathways were also enhanced in the unknown cluster, suggesting a relationship among these two clusters and confirming an association determined by pseudotime trajectory finding when all clusters were analyzed (Fig. 6*A*).

NOTCH2 influences gene expression and cluster distribution in BMMs

Independent clustering analysis of control and *Notch2*$^{tm1.1Ecan}$ BMMs treated either with M-CSF alone or M-CSF and RANKL for 3 days using UMAP for nonlinear dimensional reduction revealed the presence of the osteoclast cluster only in BMMs treated with M-CSF and RANKL (Fig. 8). A 27% increase in cells expressing genes associated with the osteoclast cluster and a 98% increase in the number of cells in the unknown cluster were observed in *Notch2*$^{tm1.1Ecan}$ BMMs when compared to control cultures. As noted, IPA revealed enhancement of similar canonical pathways in the osteoclast and unknown cluster (Fig. 7). There was increased expression of genes associated with osteoclast progenitors and precursors in *Notch2*$^{tm1.1Ecan}$ BMMs treated with M-CSF and RANKL, including the expression of *Ninj1*, encoding NINJURIN1, known to regulate osteoclast development (Fig. 8) (43). The expression of *Cited2* was not particularly increased by NOTCH2 (Figs. 8 and S1). Independent pseudotime trajectory finding of control and *Notch2*$^{tm1.1Ecan}$ BMMs revealed greater connectivity between ISG expressing immune and progenitor, dendritic, CD8+ T cells, and greater connectivity between classical and intermediate monocytes in *Notch2*$^{tm1.1Ecan-}$ BMMs treated with M-CSF and RANKL (Fig. 9).

Independent analysis of gene expression among the 11 cellular clusters from BMMs treated with M-CSF revealed that ∼40% less cells expressed *Irf8*, *Bcl6*, and *Maf6*, genes encoding

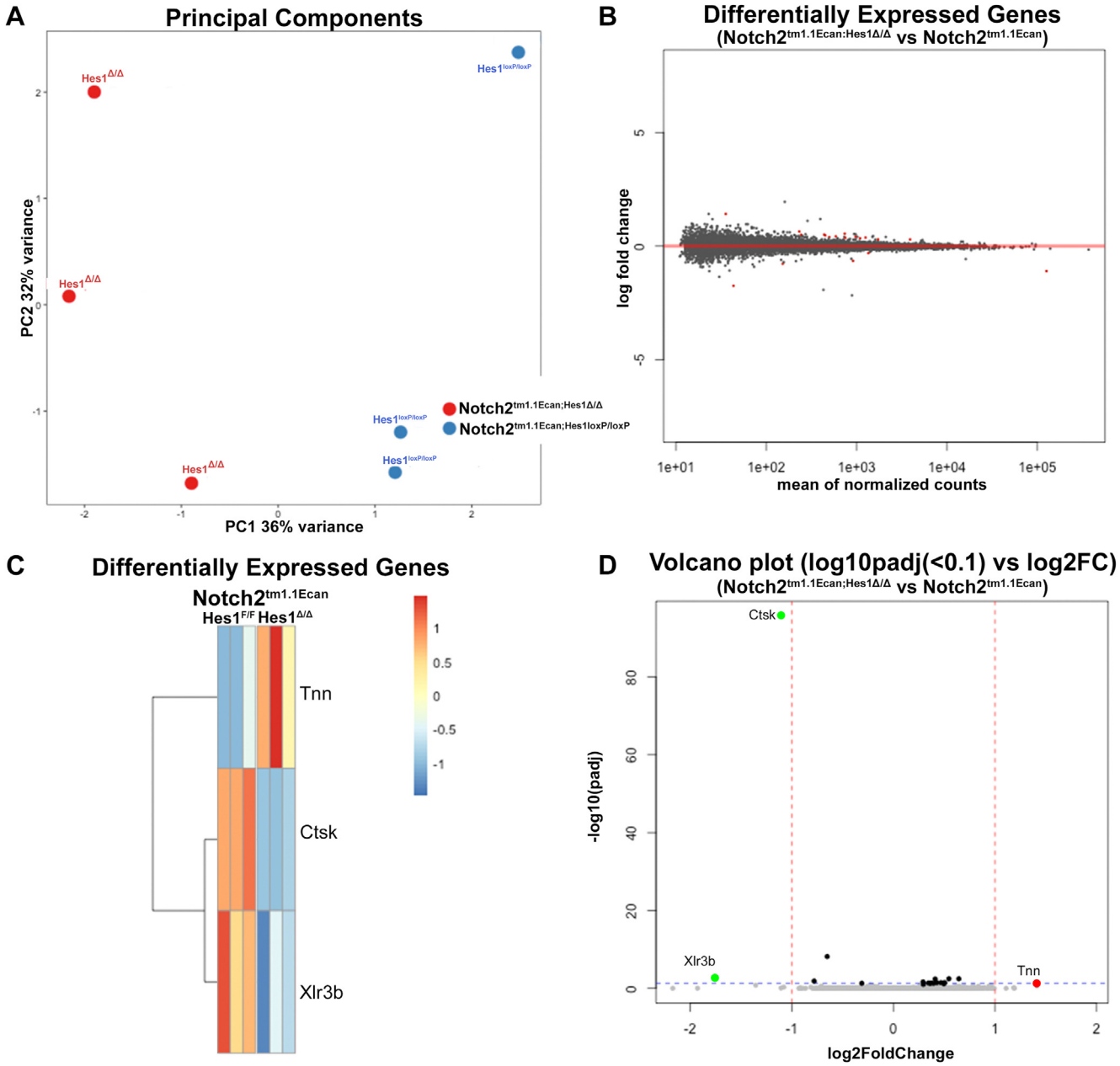

Figure 4. Transcriptional profile of osteoclasts harboring the *Hes1* deletion in the context of the *Notch2*$^{tm1.1Ecan}$ mutation. Bone marrow–derived macrophages (BMM) from 7 to 8-week-old *Notch2*$^{tm1.1Ecan}$;*Ctsk*^{Cre};*Hes1*$^{\Delta/\Delta}$ and *Notch2*$^{tm1.1Ecan}$;*Hes1*$^{loxP/loxP}$ control littermates were cultured for 4 to 5 days in the presence of M-CSF at 30 ng/ml and RANKL at 10 ng/ml. Cells were collected for total RNA and analyzed by RNA-Seq. *A*, principal component (PC) analysis of RNA-Seq replicates (n = 3 for *Hes1*$^{\Delta/\Delta}$; n = 3 for *Hes1*$^{loxP/loxP}$). *B*, differentially expressed genes as log fold change over means of normalized counts. *C*, heat map and (*D*) volcano plots of differentially expressed genes between *Notch2*$^{tm1.1Ecan}$;*Ctsk*^{Cre};*Hes1*$^{\Delta/\Delta}$ and *Notch2*$^{tm1.1Ecan}$;*Hes1*$^{loxP/loxP}$ osteoclasts log2FC false discovery rate *p* adjusted values 0.1. M-CSF, macrophage colony stimulating factor; RANKL, receptor activator of NF-κB ligand.

osteoclast inhibitors, in the osteoclast progenitor, dendritic, CD8+ T-cell cluster from *Notch2*$^{tm1.1Ecan}$ BMMs (Fig. 10). The number of cells expressing *Prdm1*, encoding B-lymphocyte-induced maturation protein 1, was increased in *Notch2*$^{tm1.1Ecan}$ in the same cluster following treatment with RANKL. Neither the number of cells nor gene expression of osteoclast inhibitors was different between *Notch2*$^{tm1.1Ecan}$ and control cultures treated with M-CSF and RANKL in the macrophage or osteoclast precursor cluster. Gene expression analysis of the osteoclast cluster from BMMs treated with M-CSF and RANKL for 3 days revealed that a greater number of cells expressing genes associated with mature osteoclasts, including *Cited2*, were present in *Notch2*$^{tm1.1Ecan}$ than in control BMMs, (Fig. 10). Although the cultures were exposed to RANKL only for 3 days, the results are congruent with enhanced osteoclastogenesis in BMMs from *Notch2*$^{tm1.1Ecan}$ mice. A complete list of genes differentially regulated in *Notch2*$^{tm1.1Ecan}$ and control BMMs is included in Table S4.

Discussion

Previous work demonstrated that NOTCH2 enhances osteoclastogenesis and mutations associated with a gain-of-

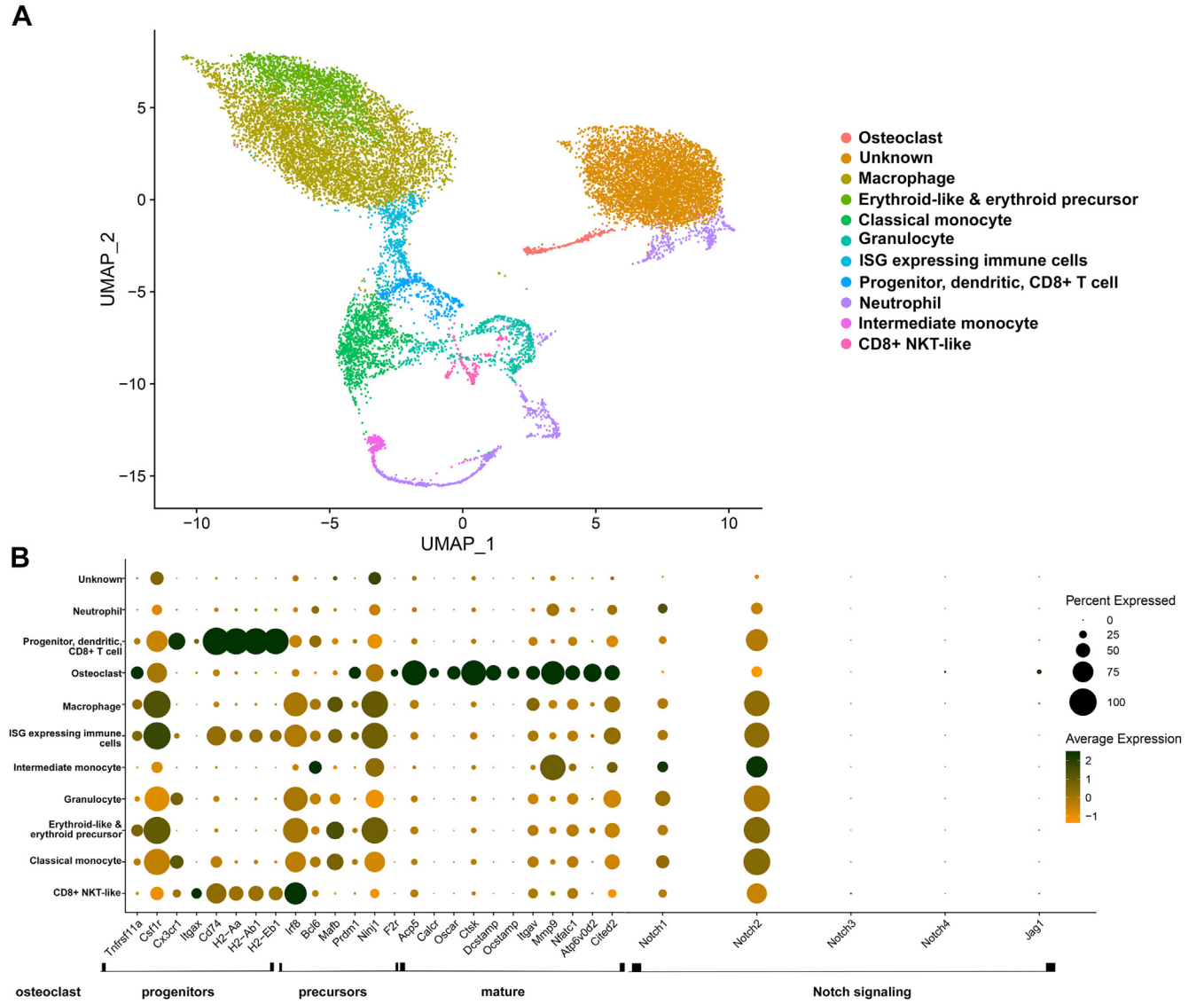

Figure 5. Uniform manifold approximation and projection for dimension reduction of scRNA-Seq data of bone marrow–derived macrophages from control and *Notch2*$^{tm1.1Ecan}$ mice reveals 11 cell clusters. *A*, UMAP visualization of 11 cell clusters of pooled normalized data from control and *Notch2*$^{tm1.1Ecan}$ BMMs cultured in the presence of M-CSF at 30 ng/ml or M-CSF at 30 ng/ml and RANKL at 10 ng/ml for 3 days. *B*, dot plot displaying the expression of genes associated with osteoclast progenitors, precursors, mature cells, and components of Notch signaling among 11 cellular clusters. *Green* denotes higher and *yellow* denotes lower than average expression, and the size of the circle represents the percentage of cells expressing each gene. BMM, bone marrow–derived macrophage; M-CSF, macrophage colony stimulating factor; RANKL, receptor activator of NF-κB ligand; UMAP, uniform manifold approximation and projection.

NOTCH2 function cause osteopenia due to increased bone resorption in mice, a phenotype that is mostly mediated by HES1 (6, 8). NOTCH1 and NOTCH2 are the prevalent Notch receptors detected in the osteoclast lineage, and whereas NOTCH2 enhances, NOTCH1 inhibits osteoclastogenesis (1, 2). Notch signaling, in particular NOTCH2 signaling, plays a role in basal M-CSF/RANKL-dependent osteoclastogenesis and γ-secretase inhibitors, known to prevent Notch activation, as well as anti-NOTCH2 antibodies targeting the NRR, known to prevent the specific activation of NOTCH2, decrease this process (4, 44). The present study extends previous observations and explores possible mechanisms responsible for the enhanced osteoclastogenesis in the context of a NOTCH2 gain-of-function. We demonstrate that NOTCH2 has a pronounced stimulatory effect on osteoclast differentiation and confirm that *in vitro*, this is mediated by HES1, since the deletion of *Hes1* in *Ctsk*-expressing cells decreases the osteoclastogenic potential of preosteoclasts and reverses the effect of NOTCH2 on osteoclast maturation (8). Osteoclast phenotypes and bulk RNA-Seq analysis of osteoclasts revealed that NOTCH2 enhances mitochondrial activity and metabolic processes associated with osteoclastogenesis (25–27). However, GSEA of RNA-Seq data needs to be interpreted with caution since no functional studies linking NOTCH2 signaling to mitochondrial respiration were conducted to verify GSEA results.

The initial analysis of differentially regulated genes by bulk RNA-Seq was carried out at an FDR *p* adjusted value of 0.1 and this has a relatively low threshold. RNA-Seq data of selected differentially regulated genes was verified by RT-PCR of RNA

Table 1
Number of cells per cluster in control and *Notch2*$^{tm1.1Ecan}$ (Notch2) bone marrow–derived macrophages cultured in the presence of M-CSF or M-CSF and RANKL

	M-CSF		M-CSF + RANKL		
Cluster	Control	Notch2	Control	Notch2	Cluster total
Unknown	1309	339	1331	2609	5588
Macrophage	1399	1103	1306	1490	5298
Erythroid	652	519	384	371	1926
Classical monocyte	340	185	329	388	1242
Granulocyte	140	112	186	193	631
ISG immune cell	106	68	176	167	517
Progenitor, dendritic, CD8+ T-cell	90	76	106	142	414
Neutrophil	200	144	253	396	993
Intermediate monocyte	65	43	67	72	247
CD8+ NKT	45	38	55	63	201
Osteoclast	3	0	115	146	264
Total	4349	2627	4308	6037	17,321

BMMs from 7- to 8-week-old *Notch2*$^{tm1.1Ecan}$ mice and control littermates were cultured in the presence of M-CSF (30 ng/ml) or M-CSF and RANKL (10 ng/ml) on a collagen matrix for 3 days. RNA-Seq data aligned to the mouse genome and gene and cell counting and cluster distribution were performed using Cell Ranger and Seurat after normalization and exclusion of clusters present in <1% of the cell population (except for osteoclasts) and merging of clusters with similar transcriptome identity. Cell number/cluster is shown for *Notch2*$^{tm1.1Ecan}$ (Notch2) and control BMMs treated with M-CSF or M-CSF and RANKL.

extracts and demonstrated downregulation of *Tnc* and *Tnn*, encoding tenascin C and N or W by NOTCH2. Tenascins are glycoproteins that modulate the adhesion of cells to the extracellular matrix and cell migration (45). *Tnn* and *Tnc* are expressed in bone and muscle and inhibit fibronectin-dependent cell adhesion (46, 47). Therefore, their downregulation by NOTCH2 in BMMs may be a mechanism utilized to favor cell attachment and differentiation toward a mature osteoclast.

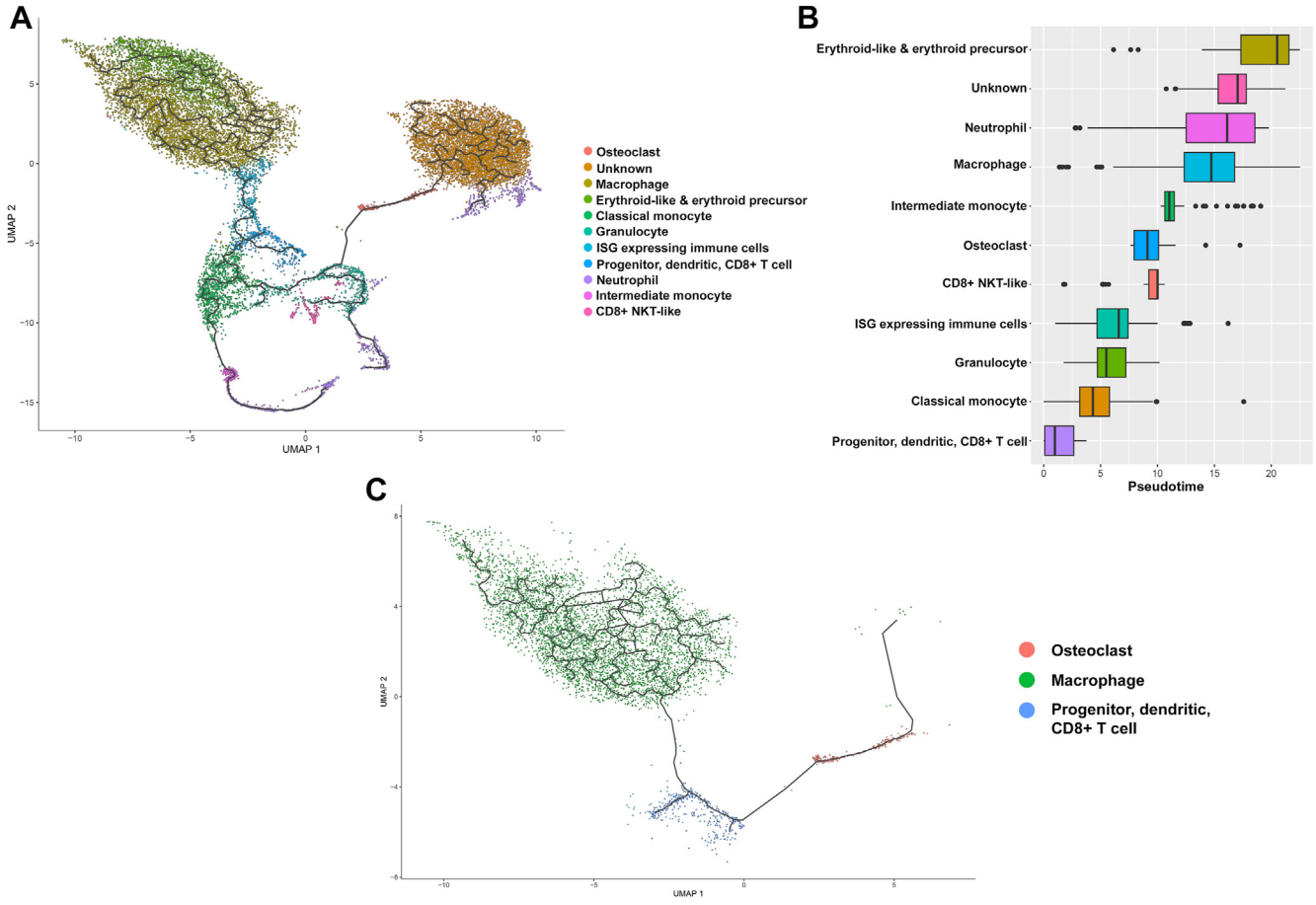

Figure 6. Trajectory analysis defines cell differentiation pathways among cell clusters identified in bone marrow–derived macrophages from control and *Notch2*$^{tm1.1Ecan}$ mice. Trajectory analysis was performed using Monocle 3 in pooled data from control and *Notch2*$^{tm1.1Ecan}$ BMMs cultured in the presence of M-CSF 30 ng/ml or M-CSF 30 ng/ml and RANKL 10 ng/ml for 3 days. *A*, trajectory analysis of the 11 cellular clusters identified. *B*, an alternative visualization of the pseudotime UMAP as a progression boxplot of pseudotime values using the progenitor cell cluster as a route node. *C*, trajectory analysis of 3 clusters related to cells of the osteoclast lineage: Memory CD8+ T-cells (progenitors), macrophages (precursor), and mature osteoclasts. BMM, bone marrow–derived macrophage; M-CSF, macrophage colony stimulating factor; RANKL, receptor activator of NF-κB ligand; UMAP, uniform manifold approximation and projection.

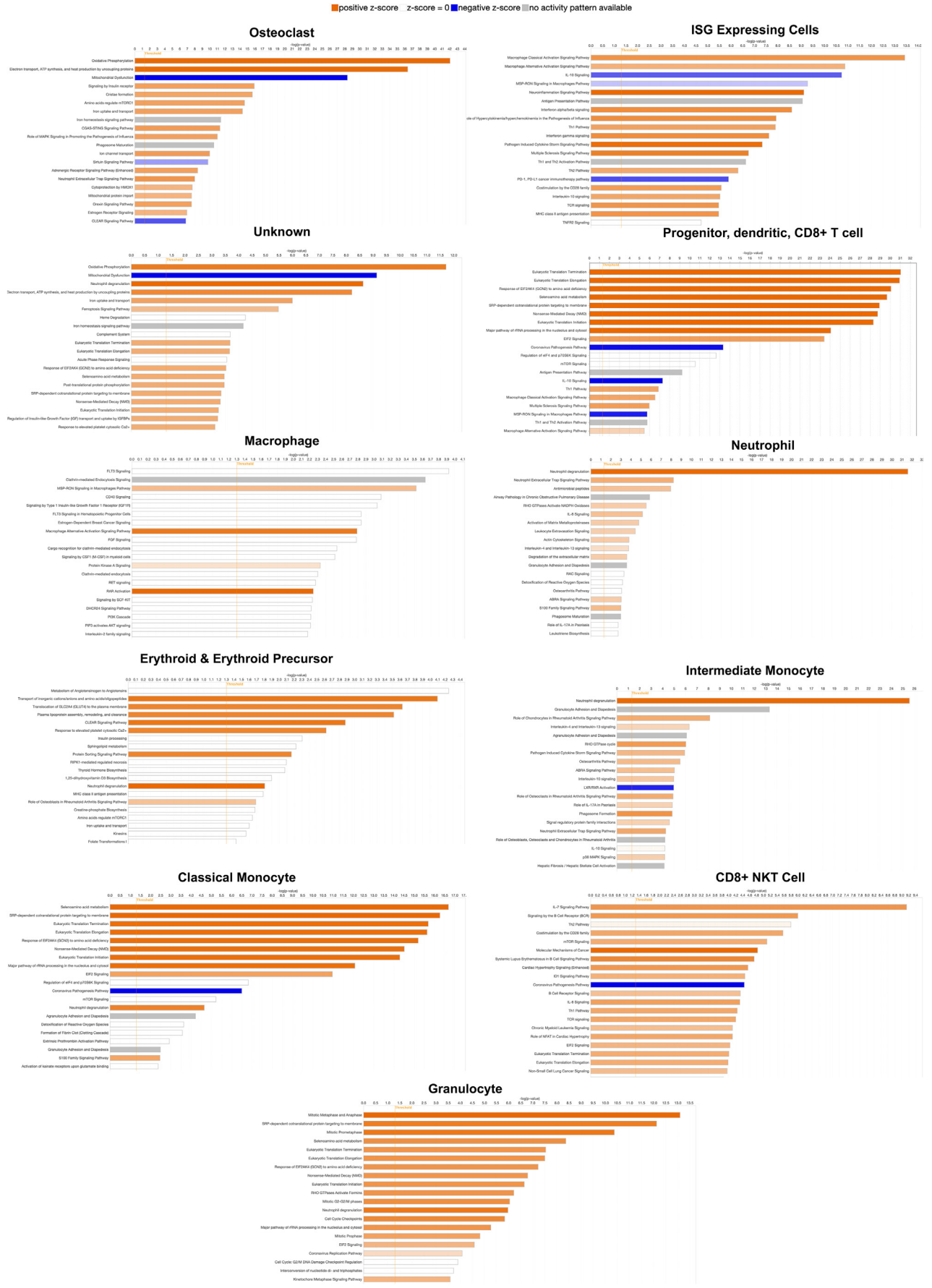

Figure 7. Mitochondrial function, oxidative respiration, and ATP synthesis are increased in the osteoclast and an "unknown cluster" from control and *Notch2*$^{tm1.1Ecan}$ bone marrow–derived macrophages. Ingenuity pathway analysis of the top 20 canonical pathways enriched in 11 cellular clusters

Previous work has demonstrated that HES1 has a pronounced effect on osteoclast differentiation and function *in vitro* and *in vivo* (8). The *Hes1* inactivation in *Ctsk*-expressing cells caused an increase in bone volume/total volume in mice, and the induction of HES1 in *Ctsk*-expressing cells caused an osteopenic phenotype (8). In the present studies, we confirm the contributory role of HES1 to osteoclastogenesis and demonstrate that in the context of the *Hes1* deletion, NOTCH2 does not enhance mitochondrial of metabolic activity during osteoclastogenesis. We also confirm that other Notch target genes, such as *Hey1*, *Hey2*, and *Heyl*, are not detected in cells of the myeloid lineage and as a consequence could not be responsible for the effects of Notch signaling in this cellular environment (3). *Notch1* and *Notch2*, but not *Notch3* and *Notch4*, were detected in multiple cellular clusters from BMM cultures confirming that NOTCH1 and NOTCH2 are the Notch receptors with the potential to influence myeloid lineage cell behavior and differentiation (3, 5). JAGGED1 was the only Notch ligand detected in the BMM environment (3).

To explore the molecular process occurring during osteoclastogenesis, we performed scRNA-Seq analysis of BMMs from *Notch2*$^{tm1.1Ecan}$ and control littermates treated with either M-CSF or M-CSF and RANKL for 3 days. The use of scRNA-Seq in combination with bulk RNA-Seq allowed us to complement the advantages of both techniques to analyze the transcriptome of BMMs in the context of a NOTCH2 gain-of-function. scRNA-Seq was particularly useful in the analysis of a complex cell culture model allowing us to discern the transcriptome profile of various cell populations present in BMM cultures treated with M-CSF or M-CSF and RANKL. It also allowed the study of NOTCH2-dependent changes in cell composition and how these changes modulate osteoclastogenesis.

Single cell RNA-Seq analysis revealed cellular heterogeneity in BMM cultures confirming prior observations in a similar culture model (24). We identified 11 cell clusters and pseudotime trajectory analysis revealed an association between clusters expressing gene markers identified in osteoclast progenitors and a cluster expressing genes associated with osteoclast precursors and a cluster expressing genes present in mature cells. This potential progression was enhanced by NOTCH2 so that a greater number of mature osteoclasts was detected in *Notch2*$^{tm1.1Ecan}$ BMMs cultured in the presence of M-CSF and RANKL than in control cultures. It is of interest that pseudotime trajectory analysis identified an unknown cluster associated with mature osteoclasts and IPA revealed that similar signaling pathways were affected in the unknown and in the osteoclast cluster. These included enhanced mitochondrial and metabolic activity, suggesting an association of the unknown cluster with osteoclast maturation. A cluster with cells displaying a gene profile associated with osteoclast progenitors, also contained dendritic and CD8+ T-cells. The latter are not known to participate in the osteoclast differentiation program. It is important to note that the cell population of each cluster is related but not necessarily completely homogeneous. In addition, murine tissues contain a subset of specialized resident dendritic cells expressing CD8 alpha, and dendritic cells have the potential to differentiate into mature osteoclasts (48–50). Indeed, the transcriptome profile of osteoclasts is closer to that of dendritic cells than to monocytes, possibly explaining the pseudotime trajectory analysis findings (51).

Our study extends recent observations on scRNA-Seq analysis of cells of the myeloid lineage and confirms the presence of a heterogenous cell population in BMM cultures (24). We also verify the presence of stepwise cell fate decision pathways in BMMs and the existence of progenitors, as well as a pre-osteoclast and an osteoclast mature population. The latter present only following the exposure of BMMs to RANKL. Our study revealed the presence of similar cell clusters in control and *Notch2*$^{tm1.1Ecan}$ BMMs. However, cluster distribution differed, and a larger proportion of mature osteoclasts and cells in the unknown clusters were present in BMMs from *Notch2*$^{tm1.1Ecan}$ than in those from control mice. The difference in osteoclast number in *Notch2*$^{tm1.1Ecan}$ and control cultures was relatively modest since BMMs were treated with M-CSF and RANKL for 3 days only, a limited period of time to avoid multinucleation and cell attachment. As a consequence, the cells did not achieve multinucleation as mature osteoclasts do, limiting somewhat the difference between controls and *Notch2*$^{tm1.1Ecan}$ cultures.

The cell heterogeneity of the BMM culture has important implications in the interpretation of results obtained with this culture model since contaminating cells may influence osteoclastogenesis. These cells may be a source of RANKL and explain studies demonstrating osteoclastogenesis in the absence of added RANKL to the culture medium (52, 53). Although *Cited2* has been shown to be required for osteoclastogenesis, its level of expression is relatively low, and it was not upregulated in the context of the NOTCH2 gain-of-function (24). Importantly, *Ninj1*, encoding NINJURIN1, was detected in multiple clusters and induced by the NOTCH2 gain-of-function and NINJURIN1 has been shown to be a positive regulator of osteoclast development (43).

In conclusion, a NOTCH2 gain-of-function enhances osteoclastogenesis, increases mitochondrial and metabolic activity of osteoclasts, and affects cell cluster allocation in BMMs.

Experimental procedures

Genetically modified mice

Notch2$^{tm1.1Ecan}$ mice harboring a 6955C>T substitution in the *Notch2* locus were studied in a C57BL/6 background (4, 44, 54). *Hes1*$^{loxP/loxP}$ (*Hes1*<*tm1Imayo*) mice, where *loxP* sequences are knocked into the first intron and downstream of the 3′ UTR of *Hes1* alleles, were obtained from RIKEN (RBRC06047; Wako Saitama) in a C57BL/6 background (55).

obtained by UMAP visualization of pooled data from control and *Notch2*$^{tm1.1Ecan}$ BMMs cultured in the presence of M-CSF 30 ng/ml or M-CSF 30 ng/ml and RANKL 10 ng/ml for 3 days. BMM, bone marrow–derived macrophage; M-CSF, macrophage colony stimulating factor; RANKL, receptor activator of NF-κB ligand; UMAP, uniform manifold appreciation and projection.

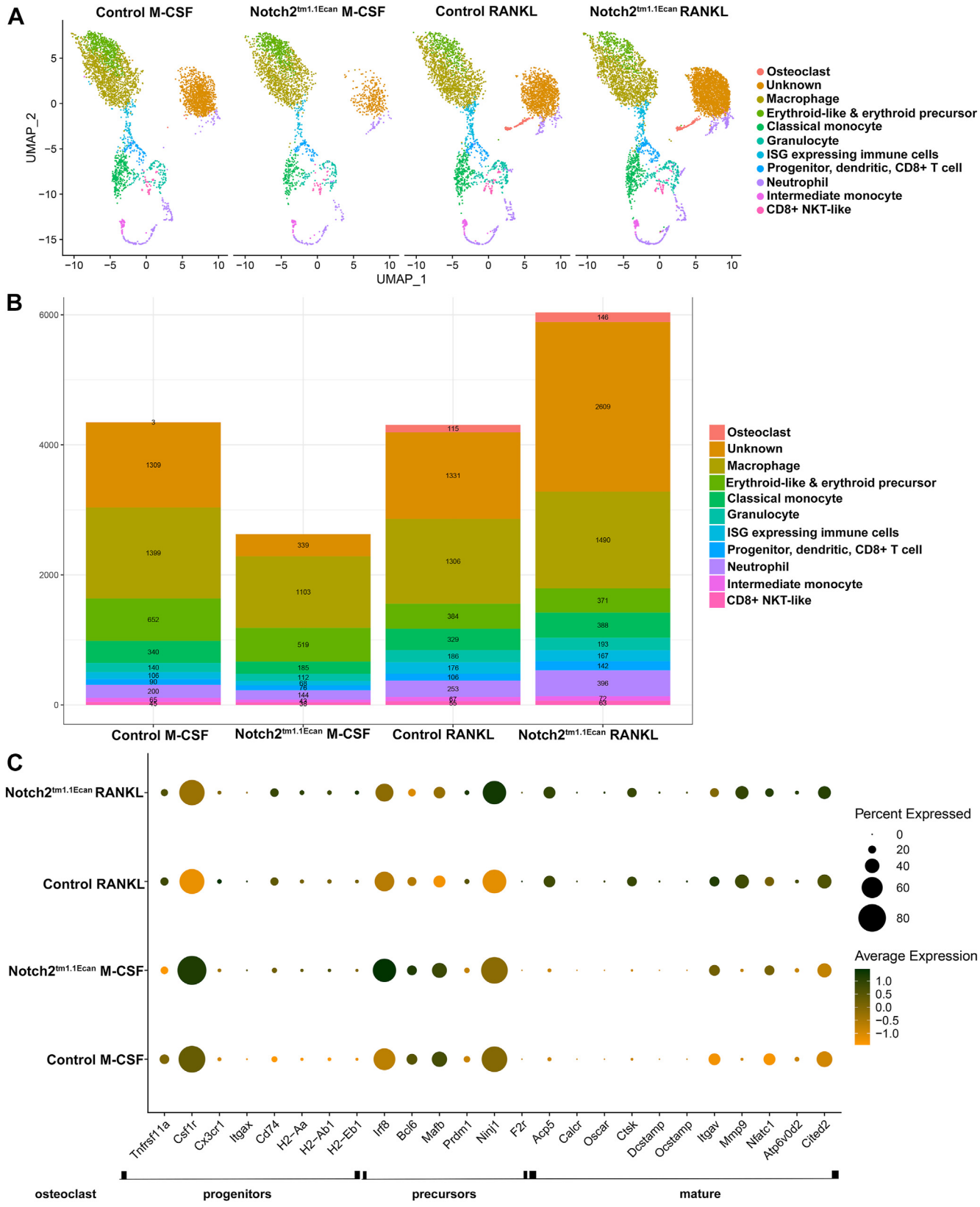

Figure 8. Uniform manifold appreciation and projection for dimension reduction reveals distinct cellular cluster distribution among bone marrow–derived macrophages from either control or *Notch2*$^{tm1.1Ecan}$ mice. *A*, UMAP visualization of 11 cell clusters of normalized data from control and *Notch2*$^{tm1.1Ecan}$ BMMs cultured in the presence of either M-CSF at 30 ng/ml or M-CSF at 30 ng/ml and RANKL at 10 ng/ml for 3 days. *B*, bar graphs demonstrate cell number present in each individual cluster from control and *Notch2*$^{tm1.1Ecan}$ BMMs treated with either M-CSF or M-CSF and RANKL. *C*, dot plot displaying the expression of genes associated with osteoclast progenitors, precursors, and mature cells in *Notch2*$^{tm1.1Ecan}$ or control BMMs treated either with M-CSF or M-CSF and RANKL. *Green* denotes higher and *yellow* denotes lower than average expression, and the size of the circle represents the percentage of cells expressing each gene. BMM, bone marrow–derived macrophage; M-CSF, macrophage colony stimulating factor; RANKL, receptor activator of NF-κB ligand; UMAP, uniform manifold approximation and projection.

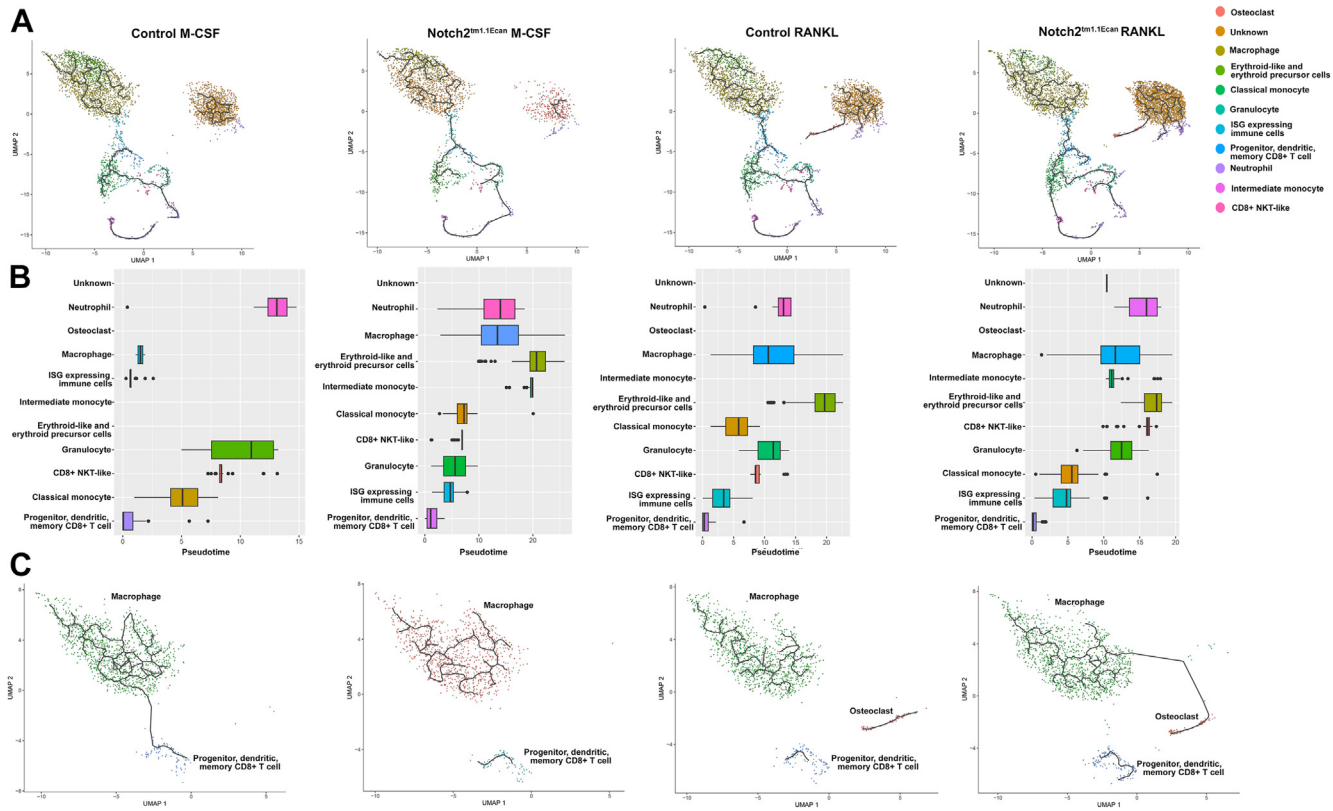

Figure 9. Trajectory analysis defines cell differentiation pathways among cell clusters identified in bone marrow–derived macrophages from control and *Notch2*$^{tm1.1Ecan}$ mice. Trajectory analysis was performed using Monocle 3 in independent single cell RNA-Seq data from control and *Notch2*$^{tm1.1Ecan}$ BMMs cultured either in the presence of M-CSF 30 ng/ml or M-CSF 30 ng/ml and RANKL 10 ng/ml for 3 days. *A*, trajectory analysis of the 11 cellular clusters identified. *B*, an alternative visualization of the pseudotime UMAP as a progression boxplot of pseudotime values using the progenitor cell cluster as a route node. *C*, trajectory analysis of 3 clusters related to cells of the osteoclast lineage: Memory CD8+ T-cells (progenitors), macrophages (precursor), and mature osteoclasts. BMM, bone marrow–derived macrophage; M-CSF, macrophage colony stimulating factor; RANKL, receptor activator of NF-κB ligand; UMAP, uniform manifold approximation and projection.

To delete *Hes1* in osteoclasts, mice harboring sequences coding for the Cre recombinase knocked-in into the *Ctsk* locus (*Ctsk*^{Cre}) were used in a C57BL/6 background (56, 57). For the deletion of *Hes1* in the context of the *Notch2*$^{tm1.1Ecan}$ mutation, *Ctsk*$^{Cre/WT}$;*Hes1*$^{loxP/loxP}$ mice were crossed with *Notch2*$^{tm1.1Ecan}$;*Hes1*$^{loxP/loxP}$ mice to create *Notch2*$^{tm1.1Ecan}$; *Ctsk*$^{Cre/WT}$;*Hes1*$^{\Delta/\Delta}$, and *Notch2*$^{tm1.1Ecan}$;*Hes1*$^{loxP/loxP}$ controls. Genotyping was conducted in tail DNA extracts by PCR using specific primers from Integrated DNA Technologies (IDT) (Table S5). Recombination of *loxP* flanked sequences was documented in extracts from tibiae using specific primers (Table S5). All animal experiments were approved by the Institutional Animal Care and Use Committee of UConn Health.

BMM cultures and osteoclast formation

To obtain BMMs, the bone marrow from 7- to 8-week-old experimental and control sex-matched littermate mice was removed by flushing with a 26-gauge needle and erythrocytes were lysed in 150 mM NH_4Cl, 10 mM $KHCO_3$, and 0.1 mM EDTA (pH 7.4), as described previously (7, 8). Cells were centrifuged and the sediment suspended in α-minimum essential medium (α-MEM; Thermo Fisher Scientific) in the presence of 10% fetal bovine serum (FBS; Atlanta Biologicals) and recombinant human M-CSF at 30 ng/ml. M-CSF complementary DNA (cDNA) and expression vector were obtained from D. Fremont and M-CSF was purified as previously reported (58). Cells were seeded on uncoated plastic petri dishes at a density of 300,000 cells/cm^2 and cultured for 3 days. For osteoclast formation, cells were collected following the addition of 0.25% trypsin/EDTA for 5 min and seeded on tissue culture plates at a density of 62,500 cells/cm^2 in α-MEM with 10% FBS, M-CSF at 30 ng/ml, and recombinant murine RANKL at 10 ng/ml. *Tnfsf11*, encoding RANKL, cDNA expression vector was obtained from M. Glogauer, and glutathione S transferase–tagged RANKL was expressed and purified as described (59). Cultures were carried out until multinucleated tartrate resistant acid phosphatase (TRAP)-positive cells were formed. TRAP enzyme histochemistry was conducted using a commercial kit (Sigma-Aldrich), in accordance with manufacturer's instructions. TRAP-positive cells containing more than three nuclei were considered osteoclasts.

For single cell RNA-Seq, BMMs from control or *Notch2*$^{tm1.1Ecan}$ mice were cultured on uncoated plastic culture dishes in the presence of M-CSF at 30 ng/ml and then seeded on culture plates previously coated with Cellmatrix Type I-A Collagen (FUJIFILM, Wako Chemicals). Cells were grown in α-MEM supplemented with 10% FBS in the presence of either M-CSF at 30 ng/ml alone or M-CSF and RANK-L at 10 ng/ml for 3 days. Four biological replicates for each experimental

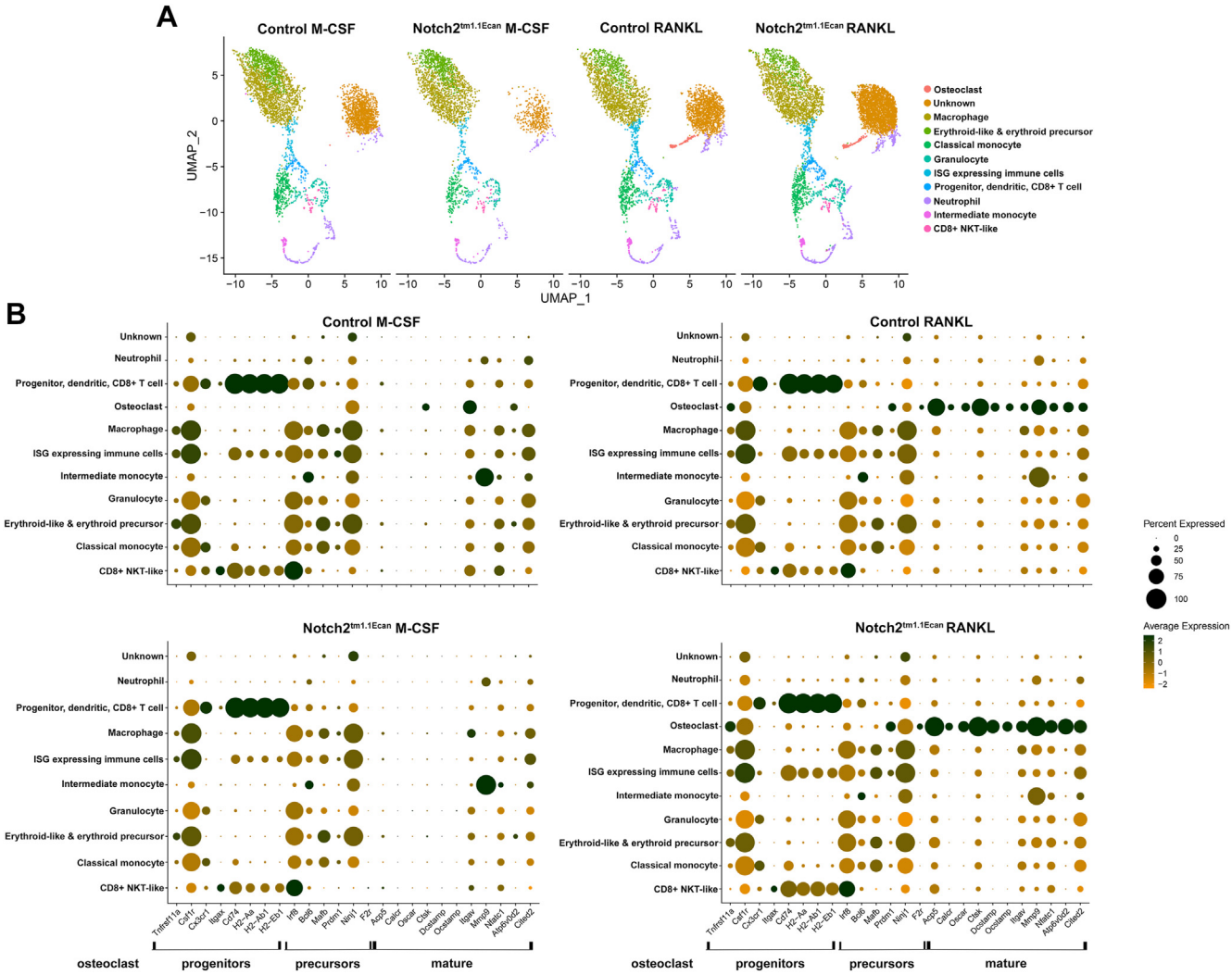

Figure 10. Differential gene expression in distinct cellular clusters from bone marrow–derived macrophages from either control or *Notch2*$^{tm1.1Ecan}$ mice. *A*, UMAP visualization of 11 cell clusters of normalized data from control and *Notch2*$^{tm1.1Ecan}$ BMMs cultured in the presence of either M-CSF at 30 ng/ml or M-CSF at 30 ng/ml and RANKL at 10 ng/ml for 3 days. *B*, dot plot displaying the expression of genes associated with osteoclast progenitors, precursors, and mature cells among 11 cellular clusters present in control or *Notch2*$^{tm1.1Ecan}$ cultures treated either with M-CSF or M-CSF and RANKL. There was no osteoclast cluster in *Notch2*$^{tm1.1Ecan}$ and only 3 osteoclasts in control cultures treated with M-CSF. *Green* denotes higher and *yellow* denotes lower than average expression, and the size of the circle represents the percentage of cells expressing each gene. To facilitate the visualization of the clusters used to generate (*B*), (*A*) is a reuse of Fig. 8*A*. BMM, bone marrow–derived macrophage; M-CSF, macrophage colony stimulating factor; RANKL, receptor activator of NF-κB ligand; UMAP, uniform manifold appreciation and projection.

condition were cultured. The collagen gel was digested with 0.1% collagenase for 15 min and cells were collected, biological replicates for each experimental condition were pooled, and processed for single cell RNA-Seq.

Real time RT-PCR

Total RNA was extracted with the RNeasy Mini kit (Qiagen). Equal amounts of RNA were reverse-transcribed using the iScript RT-PCR kit (Bio-Rad) and amplified in the presence of specific primers (all from IDT) with the SsoAdvanced Universal SYBR Green Supermix (Bio-Rad) at 60 °C for 40 cycles (Table S6). Transcript copy number was estimated by comparison with a serial dilution of cDNA for *Ctsk*, *Notch2* (both from Thermo Fisher Scientific), or *Hes1* (American Type Culture Collection, ATCC).

The level of *Notch2*$^{6955C>T}$ mutant transcript was measured as described previously (4). Total RNA was reverse transcribed with Moloney murine leukemia virus reverse transcriptase in the presence of reverse primers for *Notch2* (5′-GGATCTGG-TACATAGAG-3′) and *Rpl38* (Table S4). *Notch2* cDNA was amplified by qPCR in the presence of TaqMan gene expression assay mix, including specific primers (5′-CATCGTGACTTT CCA-3′ and 5′-GGATCTGGTACATAGAG-3′) and a 6-carboxyfluorexcein-labeled DNA probe of sequence 5′-CATTGCCTAGGCAGC-3′ covalently attached to a 3′-minor groove binder quencher (Thermo Fisher Scientific) and SsoAdvanced Universal Probes Supermix (Bio-Rad) at 60 °C for 45 cycles (60). *Notch2*$^{6955C>T}$ transcript copy number was estimated by comparison with a serial dilution of a synthetic DNA fragment (IDT) containing ∼200 bp surrounding the 6955C>T mutation in the *Notch2* locus and cloned into

pcDNA3.1(–) (Thermo Fisher Scientific) by isothermal single reaction assembly using commercially available reagents (New England Biolabs) (61).

Amplification reactions were conducted in CFX96 qRT-PCR detection systems (Bio-Rad), and fluorescence was monitored at the end of the elongation step during every PCR cycle. Data are expressed either as copy number or as relative to control mRNA normalized to 1, both corrected for *Rpl38* expression estimated by comparison to a serial dilution of cDNA for *Rpl38* (ATCC) (62).

Library preparation, bulk RNA-Seq, and bioinformatics analysis

Total RNA was quantified, and purity ratios were determined for each sample using a NanoDrop 2000 spectrophotometer (Thermo Fisher Scientific). To assess RNA quality, total RNA was analyzed on the Agilent TapeStation 4200 (Agilent Technologies) using the RNA High Sensitivity assay. RNA integrity numbers were recorded and only samples with RNA integrity numbers values above 9.0 were used for library preparation. Samples were processed for mRNA-Sequencing using the Illumina TruSeq Stranded mRNA sample preparation kit following the manufacturer's protocol (Illumina). Libraries were validated for length and adapter dimer removal using the Agilent TapeStation 4200 D1000 High Sensitivity assay (Agilent Technologies), quantified, and normalized using the dsDNA High Sensitivity Assay for Qubit 3.0 (Thermo Fisher Scientific). Sample libraries were prepared for Illumina sequencing by denaturing and diluting the libraries per manufacturer's protocol (Illumina). All samples were pooled into one sequencing pool, equally normalized, and run across the Illumina NextSeq 500 using version 2.5 chemistry. Target read depth was achieved for each sample with paired end 75 bp reads. Raw reads were trimmed with Sickle (Version 1.33), with a quality threshold of 30 and length threshold of 45 and mapped to *Mus musculus* genome (GRCm39 ensembl release 105) with HISAT2 (version 2.1.0) (63). The resulting SAM files converted into BAM format using samtools (version 1.9), and the PCR duplicates were removed using PICARD (64). The counts were generated against the features with HTSeq-count (65). The differential expression of genes between conditions was evaluated using DESeq2 (66). Covariates were introduced in the DESeq2 analysis to increase the accuracy of results, and genes showing less than 10 counts across the compared samples were excluded from the analysis. Genes with an FDR adjusted p value <0.1 were considered significant and used in the downstream analysis, as indicated in text and legends. Highly variable functions were identified and linear dimensional reduction conducted by principal component analysis. The processed RNA-Seq results were analyzed by using GSEA and by the R package clusterProfiler enrichment tool (28–31).

Single cell RNA-Seq and computational analysis

Molecular profiling at a single cell resolution was conducted on BMM cultures from *Notch2*$^{tm1.1Ecan}$ and control littermate mice. Transcriptomes were analyzed on a cell-by-cell basis through the use of microfluidic partitioning to capture single cells, and barcoded libraries were prepared using a Chromium iX instrument and Chromium Single Cell 3′ library and Gel Bead Kit V3.1 (10x Genomics). A standard throughput single gene expression kit with a cell capture efficiency of ∼65% and capable of recovering 500 to 10,000 cells/lane was used. Following reverse transcription, libraries were sequenced at the UConn Center for Genome Innovation. cDNAs from a single cell had the same barcode, allowing the sequencing reads to be mapped backed to the cell of origin (67).

FASTQ files generated using reference genome mm10-2020-A were analyzed using Cell Ranger v7.0 (10x Genomics) for sample demultiplexing, barcode processing, and counting of transcripts and output HTMLs for sample visualization and data quality assessment. Output files were used for secondary analyses, such as dimensionality reduction, cell clustering, and differential gene expression and these were performed using the Seurat R Package (v4.3) (68, 69). Cells expressing fewer than 250 transcripts, more than 10% mitochondrial RNA and cells expressing >10,000 genes/cell were excluded manually, and the data set was normalized by employing the NormalizedData function in Seurat. Highly variable functions were identified and linear dimensional reduction conducted by principal component analysis and nonlinear dimensional reduction performed by UMAP. Doublets were identified and excluded and cell clusters were then identified by the FindClusters function in Seurat and named initially by the ScType function, immune cell category, in R (32). To ensure clarity, on two instances, the cluster name was modified based on gene expression profile. Pseudotime trajectory analysis of pooled BMMs from control and *Notch2*$^{tm1.1Ecan}$ mice treated either with M-CSF or M-CSF, and RANKL was constructed by analyzing the Seurat object in Monocle 3 (70). Monocle cell data set was constructed and the learn principal graph from the reduced dimensional space was applied using learn_graph. Cells were organized along their trajectory using Monocle plot_cells and order_cells; marker genes for each cluster were identified using Seurat's FindAllMarkers function. Gene ontology, GSEA, and Qiagen IPA of differentially expressed genes was performed on a per-cluster basis, and genes prioritized based on ontology, and relevance to transcriptional control and signaling pathways (71). IPA was performed to analyze canonical pathways under Genes and Chemicals category.

Statistics

Data are expressed as means ± SD. Statistical differences were determined by unpaired Student's t-test or two-way analysis of variance with Holm Šidák analysis for multiple comparisons.

Data availability

All data are available from the corresponding author upon reasonable request. The raw sequencing data for bulk RNA-Seq and single cell RNA-Seq were deposited in Gene Expression Omnibus (GEO). https://www.ncbi.nlm.nih.gov/geo/

query/acc.cgi?acc=GSE248137 https://www.ncbi.nlm.nih.gov/geo/query/acc.cgi?acc=GSE248138.

Supporting information—This article contains supporting information.

Acknowledgments—The authors thank D. Fremont for M-CSF cDNA, M. Glogauer for *Tnfsf11* cDNA and Mary Yurczak for secretarial support.

Author contributions—C. E. conceptualization; C. E. methodology; C. E., S. L., Y. J., and D. E. investigation; C. E. writing–original draft; C. E., S. L., and Y. J. writing–review and editing; C. E. visualization; C. E. supervision; C. E. project administration; C. E. funding acquisition; D. E. formal analysis; D. E. data curation.

Funding and additional information—This work was supported by a grant from the National Institute of Arthritis and Musculoskeletal and Skin Diseases (NIAMS) AR078149. The content is solely the responsibility of the authors and does not necessarily represent the official views of the National Institutes of Health.

Conflict of interest—The authors declare that they have no conflicts of interest with the contents of this article.

Abbreviations—The abbreviations used are: α-MEM, α-minimum essential medium; BMM, bone marrow derived macrophages; cDNA, complementary DNA; FBS, fetal bovine serum; FDR, false discovery rate; FDR, false discovery ratio; GSEA, gene set enrichment analysis; HES, Hairy Enhancer of Split; HEY, Hes-related with YRPW; IPA, ingenuity pathway analysis; M-CSF, macrophage colony stimulating factor; NRR, negative regulatory region; NICD, Notch intracellular domain; RANKL, receptor activator of NF-κB ligand; RT-PCR, real time reverse transcription polymerase chain reaction; TRAP, tartrate resistant acid phosphatase; UMAP, uniform manifold approximation and projection.

References

1. Bai, S., Kopan, R., Zou, W., Hilton, M. J., Ong, C. T., Long, F., *et al.* (2008) NOTCH1 regulates osteoclastogenesis directly in osteoclast precursors and indirectly via osteoblast lineage cells. *J. Biol. Chem.* **283**, 6509–6518
2. Yu, J., and Canalis, E. (2020) Notch and the regulation of osteoclast differentiation and function. *Bone* **138**, 115474
3. Canalis, E. (2018) Notch in skeletal physiology and disease. *Osteoporos.Int.* **29**, 2611–2621
4. Canalis, E., Schilling, L., Yee, S. P., Lee, S. K., and Zanotti, S. (2016) Hajdu Cheney mouse mutants exhibit osteopenia, increased osteoclastogenesis and bone resorption. *J. Biol. Chem.* **291**, 1538–1551
5. Canalis, E. (2020) The skeleton of lateral meningocele syndrome. *Front. Genet.* **11**, 620334
6. Canalis, E., Yu, J., Schilling, L., Yee, S. P., and Zanotti, S. (2018) The lateral meningocele syndrome mutation causes marked osteopenia in mice. *J. Biol. Chem.* **293**, 14165–14177
7. Yu, J., and Canalis, E. (2019) The Hajdu Cheney mutation sensitizes mice to the osteolytic actions of tumor necrosis factor alpha. *J. Biol. Chem.* **294**, 14203–14214
8. Yu, J., Schilling, L., Eller, T., and Canalis, E. (2021) Hairy and enhancer of split 1 is a primary effector of NOTCH2 signaling and induces osteoclast differentiation and function. *J. Biol. Chem.* **297**, 101376
9. Sanchez-Irizarry, C., Carpenter, A. C., Weng, A. P., Pear, W. S., Aster, J. C., and Blacklow, S. C. (2004) Notch subunit heterodimerization and prevention of ligand-independent proteolytic activation depend, respectively, on a novel domain and the LNR repeats. *Mol. Cell. Biol.* **24**, 9265–9273
10. Schroeter, E. H., Kisslinger, J. A., and Kopan, R. (1998) Notch-1 signalling requires ligand-induced proteolytic release of intracellular domain. *Nature* **393**, 382–386
11. Gordon, W. R., Zimmerman, B., He, L., Miles, L. J., Huang, J., Tiyanont, K., *et al.* (2015) Mechanical allostery: evidence for a force requirement in the proteolytic activation of notch. *Dev. Cell.* **33**, 729–736
12. Kovall, R. A. (2008) More complicated than it looks: assembly of Notch pathway transcription complexes. *Oncogene* **27**, 5099–5109
13. Nam, Y., Sliz, P., Song, L., Aster, J. C., and Blacklow, S. C. (2006) Structural basis for cooperativity in recruitment of MAML coactivators to Notch transcription complexes. *Cell* **124**, 973–983
14. Wilson, J. J., and Kovall, R. A. (2006) Crystal structure of the CSL-Notch-Mastermind ternary complex bound to DNA. *Cell* **124**, 985–996
15. Iso, T., Kedes, L., and Hamamori, Y. (2003) HES and HERP families: multiple effectors of the Notch signaling pathway. *J. Cell. Physiol.* **194**, 237–255
16. Kobayashi, T., and Kageyama, R. (2014) Expression dynamics and functions of Hes factors in development and diseases. *Curr. Top Dev. Biol.* **110**, 263–283
17. Iso, T., Sartorelli, V., Poizat, C., Iezzi, S., Wu, H. Y., Chung, G., *et al.* (2001) HERP, a novel heterodimer partner of HES/E(spl) in Notch signaling. *Mol. Cell. Biol.* **21**, 6080–6089
18. Canalis, E. (2018) Clinical and experimental aspects of notch receptor signaling: Hajdu-Cheney syndrome and related disorders. *Metabolism* **80**, 48–56
19. Isidor, B., Lindenbaum, P., Pichon, O., Bezieau, S., Dina, C., Jacquemont, S., *et al.* (2011) Truncating mutations in the last exon of NOTCH2 cause a rare skeletal disorder with osteoporosis. *Nat. Genet.* **43**, 306–308
20. Majewski, J., Schwartzentruber, J. A., Caqueret, A., Patry, L., Marcadier, J., Fryns, J. P., *et al.* (2011) Mutations in NOTCH2 in families with Hajdu-Cheney syndrome. *Hum. Mutat.* **32**, 1114–1117
21. Simpson, M. A., Irving, M. D., Asilmaz, E., Gray, M. J., Dafou, D., Elmslie, F. V., *et al.* (2011) Mutations in NOTCH2 cause Hajdu-Cheney syndrome, a disorder of severe and progressive bone loss. *Nat. Genet.* **43**, 303–305
22. Zhao, W., Petit, E., Gafni, R. I., Collins, M. T., Robey, P. G., Seton, M., *et al.* (2013) Mutations in NOTCH2 in patients with Hajdu-Cheney syndrome. *Osteoporos. Int.* **24**, 2275–2281
23. Canalis, E., Yu, J., Singh, V., Mocarska, M., and Schilling, L. (2023) NOTCH sensitizes the chondrocyte to the inflammatory response of tumor necrosis factor alpha. *J. Biol. Chem.* , 105372. https://doi.org/10.1016/j.jbc.2023.105372
24. Tsukasaki, M., Huynh, N. C., Okamoto, K., Muro, R., Terashima, A., Kurikawa, Y., *et al.* (2020) Stepwise cell fate decision pathways during osteoclastogenesis at single-cell resolution. *Nat. Metab.* **2**, 1382–1390
25. Park-Min, K. H. (2019) Metabolic reprogramming in osteoclasts. *Semin. Immunopathol.* **41**, 565–572
26. Da, W., Tao, L., and Zhu, Y. (2021) The role of osteoclast energy metabolism in the occurrence and development of osteoporosis. *Front. Endocrinol. (Lausanne)* **12**, 675385
27. Lemma, S., Sboarina, M., Porporato, P. E., Zini, N., Sonveaux, P., Di Pompo, G., *et al.* (2016) Energy metabolism in osteoclast formation and activity. *Int. J. Biochem. Cell Biol* **79**, 168–180
28. Mootha, V. K., Lindgren, C. M., Eriksson, K. F., Subramanian, A., Sihag, S., Lehar, J., *et al.* (2003) PGC-1alpha-responsive genes involved in oxidative phosphorylation are coordinately downregulated in human diabetes. *Nat. Genet.* **34**, 267–273
29. Subramanian, A., Tamayo, P., Mootha, V. K., Mukherjee, S., Ebert, B. L., Gillette, M. A., *et al.* (2005) Gene set enrichment analysis: a knowledge-based approach for interpreting genome-wide expression profiles. *Proc. Natl. Acad. Sci. U. S. A.* **102**, 15545–15550
30. Yu, G., Wang, L. G., Han, Y., and He, Q. Y. (2012) clusterProfiler: an R package for comparing biological themes among gene clusters. *OMICS* **16**, 284–287
31. Wu, T., Hu, E., Xu, S., Chen, M., Guo, P., Dai, Z., *et al.* (2021) clusterProfiler 4.0: a universal enrichment tool for interpreting omics data. *Innovation (Camb)* **2**, 100141

32. [preprint] McInnes, L., Healy, J., and Melville, J. (2020) UMAP: Uniform Manifold Approximation and Projection for Dimension Resolution. *arXiv*. https://doi.org/10.48550/arXiv.1802.03426
33. Dobigny, C., and Saffar, J. L. (1997) H1 and H2 histamine receptors modulate osteoclastic resorption by different pathways: evidence obtained by using receptor antagonists in a rat synchronized resorption model. *J. Cell. Physiol.* **173**, 10–18
34. Yamaura, K., Yonekawa, T., Nakamura, T., Yano, S., and Ueno, K. (2003) The histamine H2-receptor antagonist, cimetidine, inhibits the articular osteopenia in rats with adjuvant-induced arthritis by suppressing the osteoclast differentiation induced by histamine. *J. Pharmacol. Sci.* **92**, 43–49
35. Hoshino, A., Ueha, S., Hanada, S., Imai, T., Ito, M., Yamamoto, K., *et al.* (2013) Roles of chemokine receptor CX3CR1 in maintaining murine bone homeostasis through the regulation of both osteoblasts and osteoclasts. *J. Cell Sci.* **126**, 1032–1045
36. Mun, S. H., Won, H. Y., Hernandez, P., Aguila, H. L., and Lee, S. K. (2013) Deletion of CD74, a putative MIF receptor, in mice enhances osteoclastogenesis and decreases bone mass. *J. Bone Miner. Res.* **28**, 948–959
37. Nishikawa, K., Nakashima, T., Hayashi, M., Fukunaga, T., Kato, S., Kodama, T., *et al.* (2010) Blimp1-mediated repression of negative regulators is required for osteoclast differentiation. *Proc. Natl. Acad. Sci. U. S. A.* **107**, 3117–3122
38. Zhao, B., Takami, M., Yamada, A., Wang, X., Koga, T., Hu, X., *et al.* (2009) Interferon regulatory factor-8 regulates bone metabolism by suppressing osteoclastogenesis. *Nat. Med.* **15**, 1066–1071
39. Miyauchi, Y., Ninomiya, K., Miyamoto, H., Sakamoto, A., Iwasaki, R., Hoshi, H., *et al.* (2010) The Blimp1-Bcl6 axis is critical to regulate osteoclast differentiation and bone homeostasis. *J. Exp. Med.* **207**, 751–762
40. Takayanagi, H. (2005) Mechanistic insight into osteoclast differentiation in osteoimmunology. *J. Mol. Med. (Berl)* **83**, 170–179
41. Nakashima, T., Hayashi, M., and Takayanagi, H. (2012) New insights into osteoclastogenic signaling mechanisms. *Trends Endocrinol. Metab.* **23**, 582–590
42. Zhang, Y., Wang, H., Zhu, G., Qian, A., and Chen, W. (2020) F2r negatively regulates osteoclastogenesis through inhibiting the Akt and NFkappaB signaling pathways. *Int. J. Biol. Sci.* **16**, 1629–1639
43. Bae, S. J., Shin, M. W., Son, T., Lee, H. S., Chae, J. S., Jeon, S., *et al.* (2019) Ninjurin1 positively regulates osteoclast development by enhancing the survival of prefusion osteoclasts. *Exp. Mol. Med.* **51**, 1–16
44. Canalis, E., Sanjay, A., Yu, J., and Zanotti, S. (2017) An antibody to Notch2 reverses the osteopenic phenotype of hajdu-cheney mutant male mice. *Endocrinology* **158**, 730–742
45. Martina, E., Chiquet-Ehrismann, R., and Brellier, F. (2010) Tenascin-W: an extracellular matrix protein associated with osteogenesis and cancer. *Int. J. Biochem. Cell Biol.* **42**, 1412–1415
46. Pesheva, P., Probstmeier, R., Skubitz, A. P., McCarthy, J. B., Furcht, L. T., and Schachner, M. (1994) Tenascin-R (J1 160/180 inhibits fibronectin-mediated cell adhesion–functional relatedness to tenascin-C. *J. Cell Sci.* **107**, 2323–2333
47. Morgan, J. M., Wong, A., Yellowley, C. E., and Genetos, D. C. (2011) Regulation of tenascin expression in bone. *J. Cell. Biochem.* **112**, 3354–3363
48. Shortman, K., and Heath, W. R. (2010) The CD8+ dendritic cell subset. *Immunol. Rev.* **234**, 18–31
49. Neuenhahn, M., and Busch, D. H. (2007) Unique functions of splenic CD8alpha+ dendritic cells during infection with intracellular pathogens. *Immunol. Lett.* **114**, 66–72
50. Alnaeeli, M., Penninger, J. M., and Teng, Y. T. (2006) Immune interactions with CD4+ T cells promote the development of functional osteoclasts from murine CD11c+ dendritic cells. *J. Immunol.* **177**, 3314–3326
51. Gallois, A., Lachuer, J., Yvert, G., Wierinckx, A., Brunet, F., Rabourdin-Combe, C., *et al.* (2010) Genome-wide expression analyses establish dendritic cells as a new osteoclast precursor able to generate bone-resorbing cells more efficiently than monocytes. *J. Bone Miner. Res.* **25**, 661–672
52. Tanaka, S. (2017) RANKL-independent osteoclastogenesis: a long-standing controversy. *J. Bone Miner. Res.* **32**, 431–433
53. Lam, J., Takeshita, S., Barker, J. E., Kanagawa, O., Ross, F. P., and Teitelbaum, S. L. (2000) TNF-alpha induces osteoclastogenesis by direct stimulation of macrophages exposed to permissive levels of RANK ligand. *J. Clin. Invest.* **106**, 1481–1488
54. Yu, J., Zanotti, S., Walia, B., Jellison, E., Sanjay, A., and Canalis, E. (2018) The Hajdu Cheney mutation is a determinant of B-cell allocation of the splenic marginal zone. *Am. J. Pathol.* **188**, 149–159
55. Imayoshi, I., Shimogori, T., Ohtsuka, T., and Kageyama, R. (2008) Hes genes and neurogenin regulate non-neural versus neural fate specification in the dorsal telencephalic midline. *Development* **135**, 2531–2541
56. Nakamura, T., Imai, Y., Matsumoto, T., Sato, S., Takeuchi, K., Igarashi, K., *et al.* (2007) Estrogen prevents bone loss via estrogen receptor alpha and induction of Fas ligand in osteoclasts. *Cell* **130**, 811–823
57. Jacome-Galarza, C., Soung do, Y., Adapala, N. S., Pickarski, M., Sanjay, A., Duong, L. T., *et al.* (2014) Altered hematopoietic stem cell and osteoclast precursor frequency in cathepsin K null mice. *J. Cell. Biochem.* **115**, 1449–1457
58. Lee, S. H., Rho, J., Jeong, D., Sul, J. Y., Kim, T., Kim, N., *et al.* (2006) v-ATPase V0 subunit d2-deficient mice exhibit impaired osteoclast fusion and increased bone formation. *Nat. Med.* **12**, 1403–1409
59. Wang, Y., Lebowitz, D., Sun, C., Thang, H., Grynpas, M. D., and Glogauer, M. (2008) Identifying the relative contributions of Rac1 and Rac2 to osteoclastogenesis. *J. Bone Miner. Res.* **23**, 260–270
60. Kutyavin, I. V., Afonina, I. A., Mills, A., Gorn, V. V., Lukhtanov, E. A., Belousov, E. S., *et al.* (2000) 3'-minor groove binder-DNA probes increase sequence specificity at PCR extension temperatures. *Nucleic Acids Res.* **28**, 655–661
61. Gibson, D. G., Young, L., Chuang, R. Y., Venter, J. C., Hutchison, C. A., 3rd, and Smith, H. O. (2009) Enzymatic assembly of DNA molecules up to several hundred kilobases. *Nat. Methods* **6**, 343–345
62. Kouadjo, K. E., Nishida, Y., Cadrin-Girard, J. F., Yoshioka, M., and St-Amand, J. (2007) Housekeeping and tissue-specific genes in mouse tissues. *BMC Genomics* **8**, 127
63. Kim, D., Langmead, B., and Salzberg, S. L. (2015) HISAT: a fast spliced aligner with low memory requirements. *Nat. Methods* **12**, 357–360
64. Li, H., Handsaker, B., Wysoker, A., Fennell, T., Ruan, J., Homer, N., *et al.* (2009) The sequence alignment/map format and SAMtools. *Bioinformatics* **25**, 2078–2079
65. Anders, S., Pyl, P. T., and Huber, W. (2015) HTSeq–a Python framework to work with high-throughput sequencing data. *Bioinformatics* **31**, 166–169
66. Love, M. I., Huber, W., and Anders, S. (2014) Moderated estimation of fold change and dispersion for RNA-seq data with DESeq2. *Genome Biol.* **15**, 550
67. Ding, J., Smith, S. L., Orozco, G., Barton, A., Eyre, S., and Martin, P. (2020) Characterisation of CD4+ T-cell subtypes using single cell RNA sequencing and the impact of cell number and sequencing depth. *Sci. Rep.* **10**, 19825
68. Butler, A., Hoffman, P., Smibert, P., Papalexi, E., and Satija, R. (2018) Integrating single-cell transcriptomic data across different conditions, technologies, and species. *Nat. Biotechnol.* **36**, 411–420
69. Stuart, T., Butler, A., Hoffman, P., Hafemeister, C., Papalexi, E., Mauck, W. M., 3rd, *et al.* (2019) Comprehensive integration of single-cell data. *Cell* **177**, 1888–1902.e1821
70. Trapnell, C., Cacchiarelli, D., Grimsby, J., Pokharel, P., Li, S., Morse, M., *et al.* (2014) The dynamics and regulators of cell fate decisions are revealed by pseudotemporal ordering of single cells. *Nat. Biotechnol.* **32**, 381–386
71. Kramer, A., Green, J., Pollard, J., Jr., and Tugendreich, S. (2014) Causal analysis approaches in ingenuity pathway analysis. *Bioinformatics* **30**, 523–530